Experimental investigation of model piles subject to lateral load in cohesionless soil

Nabaa A. Al-Fahham[1]*and Ali A. Al-Jazaairry*[1]*

[1] Civil Engineering Department, University of Kufa, Najaf, Iraq.

Abstract. In this research work, the way piles behave in sandy soil and are exposed to lateral forces was examined experimentally by using several lab examinations. These tests were performed on a model of steel piles, including a closed-ended circular pile, a closed-ended square pile, and an H pile. The outcomes of the experimental tests were presented as load-displacement diagrams to examine how pile length and shape affected lateral load capability. Moreover, along the length of the pile, the bending moments were obtained and presented as relationships between the bending moment and the pile length. Therefore, it can be said that piles' capacity to support lateral loads rises with increasing pile length for each of the study's pile shapes. Additionally, it finds that the H-pile has a greater lateral load capacity and maximum bending moment than other piles.

1 Introduction

Pile foundations are widely employed to help constructions withstand the lateral stress loads that apply on them. Commonly used to support structures like transmission towers, high-rise buildings, and bridges, pile foundations are frequently exposed to lateral loads caused by wind, waves, earthquakes, or traffic. These constructions must satisfy two requirements in order to operate them properly. The first requirement is that the pile must be protected against ultimate failure while the second requirement is the normal deflection under operational loads must be within the allowable bound. Maximum lateral resistance of the pile is additionally required for the creation of such piles. The pile responds to lateral stresses depending on the interaction between the pile and the ground around it. Thus, the way in which piles respond to loads applied laterally is determined by the way the pile and the ground interact. The reactions of piles when they are under lateral loads is greatly impacted by the behavior of soil stress-strain, that includes the soil/pile interface, stiffness, density, and shear strength. Piles' stiffness and shape are also having significant impact on pile performance.

There are several methods for forecasting the piles' lateral load capacity in cohesionless soil. Numerous tests utilizing model piles have been conducted to determine the efficacy of piles under lateral loading. Under monotonic lateral stresses, (Mahdy et al., 2014) [1] found that the maximum bending moments increased as the relative density increased using seven levels of electrical strain gauges on the model tests that were subjected to lateral loads in Johor Bahru sand. (Salini and Girish, 2009) [2] was found that as pile length, diameter, weight, roughness, and sand density increase, so does the piles' lateral load capacity.

However, (Ghabezloo et al., 2021) [3] show that the increases the spacing to diameter and embedment ratio have been found to increase the maximum lateral load capacity of both single and multiple piles. (Mahmoud, 2021) [4] found that some of the factors that determine how piles behave under lateral stresses include their diameter, their slenderness ratio, their angle with the vertical, and the type of soil. It was noticed that increasing the diameter, slenderness ratio, and angle with the vertical increased the pile load. And as the impact of these characteristics on pile deflection has been examined through experimental research. Many factors influence a pile's lateral loading capacity, including the pile's diameter, length, material, and soil characteristics. The distribution of the load between the lateral surface and the base of the pile is influenced by the pile's diameter as presented by [5]

*Corresponding author: alia.aljazairi@uokufa.edu.iq

Moreover, it is observed the lateral bearing resistance of piles rises with increasing cross-section area, which also minimizes displacements near ground as stated by [6]. While (Jiang et al., 2023) [7] was found for the same lateral load, the rectangular piles' pile deflection is less than the circular piles. This is because the bending stiffness of the rectangular pile is greater, thereby limiting the deflection of the pile. Under similar loading conditions, rectangular piles have a greater bending moment than circular piles, and their maximum bending moment is located in a deeper

location.

(Begum and Muthukkumaran, 2009) [8] was found that when the applied lateral load increased, the maximum bending moment also increased, indicating that the pile's lateral load capacity increased as its embedment length increased. According to (Chik et al., 2009) [9] the response's lateral pile was affected by the elevation of the water table. Higher lateral resistance is produced by dry soil conditions than by fully saturated soil conditions.

In summary, various research work is presented in the literature discovering the general lateral load behavior of piles located in cohesionless soil. Because of the limited studies have been investigated experimentally cross sectional effect and slenderness ratio of piles on the lateral load capacity and the bending moment, this study aims to explore these factors thoroughly. Thus, three pile shape as well as three pile length were included in the experimental investigation of this research work to obtain their impact on pile lateral capacity as well as the bending moment throughout the pile's length.

2 Soil Properties

The sandy soil utilized in this study was taken from the city's center of Al-Najaf city in the middle of Iraq. The soil was subjected to a variety of chemical studies, including the T.D.S. test, gypsum concentration, sulfate content (SO_4), and soil organic content as shown in Table 1. However, it is essential to state that all tests in this study were in the University of Kufa / Department of Civil Engineering Laboratory.

TABLE 1. Characteristic properties of reclaimed soil

Soil property	Value	Specification
T.D.S (Total Dissolved Solids)	0.74 %	B.S 1337 PART.3
Gypsum content	4.75 %	
SO_4	2.21 %	
Organic materials	0.35 %	

Moreover, the soil was physically examined using several tests such as sieve analysis (Figure 1), field unit weight, the specific gravity, optimal moisture content (O.M.C.) and maximum density (Proctor test), Minimum Dry Unit Weight and Direct Shear Test as shown in Table 2.

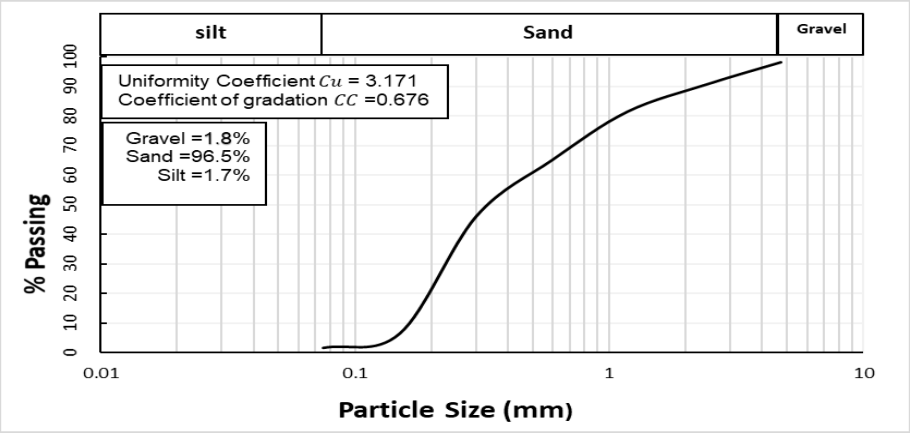

Fig 1. The grain size distribution curve of used soil

TABLE 2. Physical characteristics of the utilized soil

Soil Property	Value	Specification
Water Content of site Soil (%)	5	ASTM D 2216 – 10
Field unit weight (kN/m^3)	17.5	ASTM D 1556-07
D_{10}, (mm)	0.16	ASTM D 422-63
D_{30}, (mm)	0.24	
D_{60}, (mm)	0.52	
Coefficient of uniformity (Cu)	3.2	-
Coefficient of curvature (Cc)	0.68	-
Soil Classification	SP	Unified Soil Classification system (USCS)
Maximum dry unit weight (Procter) (kN/m^3)	18.48	ASTM D 698-07
Optimum moisture content (O.M.C), (%)	12	
Friction angle, Ø (°)	37	ASTM D 3080-7
Cohesion (kN/m^2)	4.85	
Minimum dry unit weight (kN/m^3)	15.6	ASTM D 4254-16
Specific Gravity Gs	2.67	ASTM D 854
Relative density, Dr (%)	40	-

3 Testing Apparatus

3.1 The Loading System

Two 3.5-inch channel plates that have a length of 1.5m (measured from the bottom of the box to the higher end) are fitted on the sides of the box to make up the metal frame. The main channel plate can be moved vertically up and down as needed by sliding the side channel plates, where each have 19 mm holes and a 50 mm gap between them. The upper plate has a length of 850 mm and it is likewise a channel plate. To install them with the aforementioned holes and 19 mm stainless steel bolts, the two ends are closed with 19 mm holes. Electric Jack base having two metal plates with a combined thickness of 6 mm to make up the base, which is joined to a metal tube with a 30.2 mm diameter. The upper plate is perforated for fixing with another plate on the top of the upper channel plate of the frame, which is also perforated. The bottom plate is perforated to fix the jack inside the base. According to Figure 2, it is attached to the base using stainless steel bolts that measure 19 mm in diameter and 100 mm in length each.

Fig 2. Loading unit

3.2 Pile Model

Three types of steel model piles were used: H-piles, close-ended square piles, and close-ended circular piles. The piles are exactly the same width of 25 mm. Furthermore, three slenderness ratios or length to diameter ratios L/D of 11, 14, and 17 were included to describe the pile lengths. The model pile diameter was chosen in accordance with the advice given by (Bolton et al.,1999) [17] in order to prevent the boundary and scale effects in the current experimental study. One of the guidelines is that the ratio of the container diameter to the pile diameter (D container/D pile) needs to be more than 8 in order to eliminate the wall effects while doing the model pile capacity estimation tests, Where the container walls have no effect on the influence zone around the pile [18].

3.3 Testing Box

A steel container made from 2 mm thick steel plate with dimensions of (700×700) mm was used. These dimensions were selected to eradicate the impact of boundaries conditions in the model tests. The area affected by driving a pile in cohesionless soil is between 4.5 and 5.5 times the diameter from the pile's side, according to [19]. However, in the current study the distance between the pile and the wall of the container is 14 times more than the pile diameter which is clearly more the recommended ratio. The height of the steel container was 800 mm. According to the earlier studies, the driving pile's influence in the cohesiveness soil should reach 3 to 4.5 times its diameter below the pile tip, [19]. This depth was chosen to reflect this guideline. The box was divided into eight layers from the inside with distinct lines to guarantee that the required soil density was obtained during the soil filling process.

3.4 Sand Density Control Technique

The amount of soil required for each layer depends on the density required for the test which is the density utilized throughout the testing process that is similar to the field density of 17.5 kN/m^3. After calculating the weight of soil essential for each layer, the soil's water content is verified by microwave before being compacted in the box. Three samples are taken for each stratum in accordance with ASTM D-4643 specifications, and the water content is examined in each sample. After confirming the water content, soil is added to fill a layer. Lines separating the interior side of the soil box are utilized to clearly identify the strata. The soil for each layer should be added, then the surface should be leveled and compacted to the required density.

3.5 The Measuring System

A screw hydraulic jack that applied a maximum load of 500 kg and is connected to a control system for controlling the jack makes up the loading system. This technique enables control of both the jack movement and the direction of loading, allowing compressive loading to be applied to the pile. To provide consistent electricity while applying the load, the jack is attached to a small motor. A small motor is connected to a power source, and the voltage regulator that powers the motor maintains steady throughout the duration of the test. A bolt with a diameter of 18 mm and a length of 110 mm is

fastened to the jack's end and the load cell is affixed to the second side of this bolt for recording the applied load. To measure the pile's movement, Differential Linear Variable Transformer LVDT was used. Further, on the outer surface of the model piles with slenderness ratio of 14, There were five strain gauges (SG) fastened to read the strains along the model pile. These strain reading are converted to bending moment values by multiplying them by certain factors. These factors were obtained from specific tests by fixing the model piles from one end and applying known load on another end which makes the model pile act as a cantilever beam. Additionally, a data collection LabVIEW software was used to record and store all of the readings from strain gauges, LVDT, and load cell. The development environment and platform for a visual programming language are called LabVIEW from National Instruments. A Laboratory Virtual Instrumentation Engineering Workbench defines what LabVIEW means. Before the tests began, the devices were calibrated, and the data was transmitted as tables for processing by the computer. A testing system schematic diagram is shown in Figure 3.

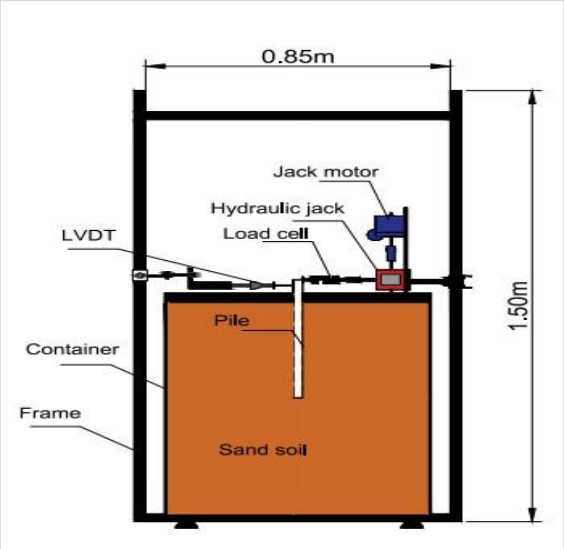

Fig3. The testing system's schematic diagram

4 Experimental Program

4.1 Preparing the Soil and Installing the Model Pile

The soil is prepared for achieving the required soil unit weight of 17.5 kN/m^3. Then selecting the pile model (type and slenderness ratio) to be tested. The model pile is installed by the temporary pile holder and the container is filled by sand layers until the soil reaches the container's top. Afterward, the pile holder is removed and then the LVDT is installed and the loading head is set on the pile. This process is repeated for each pile shape and slenderness ratio.

4.2 Pile Testing

The loading system is fixed to the testing frame. Then, the LVDT is installed to measure the horizontal displacement after applying a side compression force gradually by means of a hydraulic jack, where it records the pile's displacement after the load is applied with the load placed on the data recorder. Figure 4 illustrates the loading of the pile.

Fig 4. Testing of the pile

5 Experimental Results and Discussion

To evaluate the pile's bearing capacity, a total of nine lateral loading tests were performed for three slenderness ratios. The pile's applied load had been measured during the tests by a load cell, and the pile's movement was measured by LVDT. These variables affect the pile's bearing capacity and its resistance to failure. The parameters involved in this study are the pile shape and length of the pile, the bearing capacity of the pile, and the bending moment generated by the lateral load. The following sections show the changes in lateral displacement of the pile with the lateral load created for each of the testing conditions. The nonlinear load-displacement curves behave similarly. The impact of pile length and pile shape was examined using the lateral load versus lateral displacement graphs. The value of load at which there is a peak on the curve or the load where the curve continues to move continuously in the load-displacement graph were all used to determine the piles' ultimate lateral load capacity [21].

6 Effect of Pile Shape

6.1 Ultimate Pile Capacity for Slenderness ratio of 11

The static load test results were utilized to assess the values of ultimate pile capacity (Qu). The static load test has been carried out in order to determine the amount of loading required to attain the pile's maximum load capacity while testing the pile models under lateral load. The curves of load-settlement for every type of pile are displayed in Figure 5. Comparing the values of Qu for the H-pile to the close-ended square pile and close-ended circular pile, respectively, shows increases in pile capacity of 8.3% and 18.2%. Comparing to the other pile shapes, the H-pile experiences more densification during the pressing process.

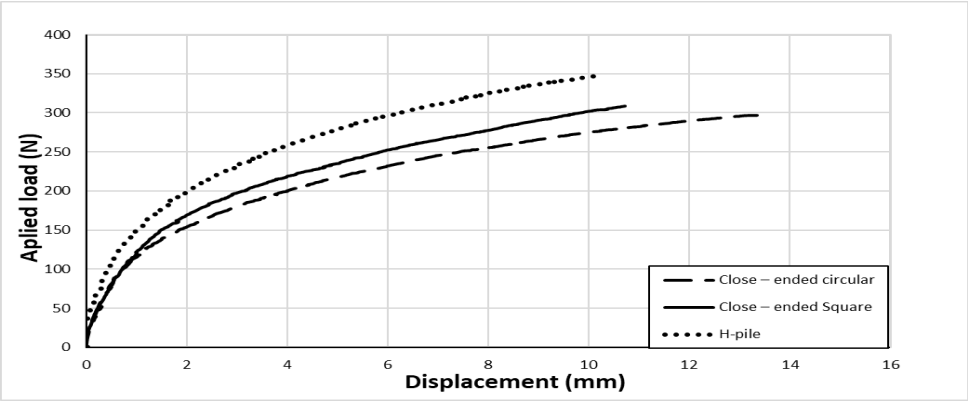

Fig 5. Load- displacement curves for different shapes of piles with L/D =11

6.2 Ultimate Pile Capacity for Slenderness ratio of 14

Figure 6 reveals The curves of load- displacement for different shapes of piles. The values of pile capacities were established using the static load tests. It is clear that the H-pile had a larger displacement value than the close-ended circular and square piles (from 0 to 300 N). The H-pile curve started moving at loading equals to 100 N where the curve until this value has no displacement of the pile head. After this point of 100 N load the pile head started moving due to the application of the lateral load. According to the findings, the values of the pile capacity of H-pile increased by 17.4% and 8%, respectively, in comparision with close-ended circular and square piles. The values of pile capacity were 1.17 times higher for an H-pile than for a closed-ended circular pile. This may be the sand available along the pile's length. Thus, increasing the contact surface area and increasing recorded skin friction. This is apparently from the close-ended pile applied loads that were recorded and shown in Figure 6.

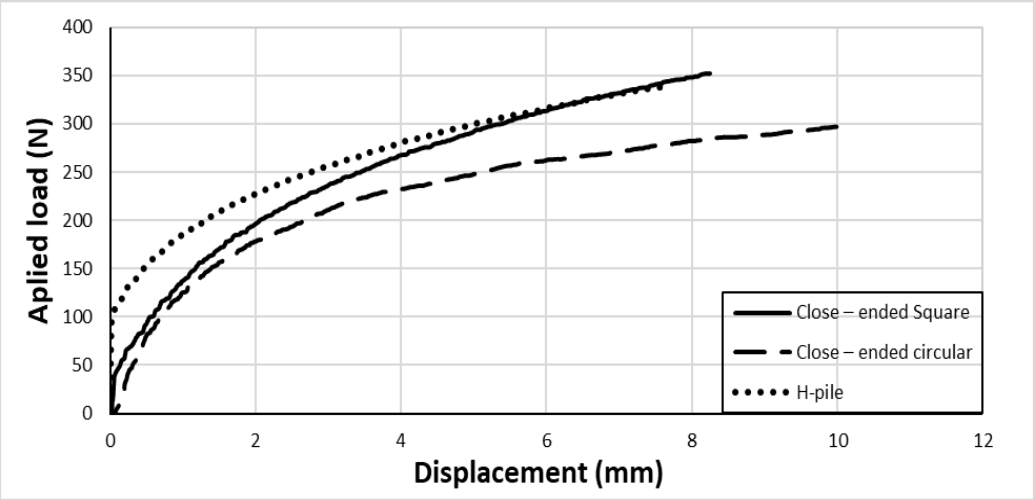

Fig 6. Load - displacement curves for different shapes of piles with L/D =14

6.3 Ultimate Pile Capacity for Slenderness ratio of 17

Figure 7 depicts the applied load for a variety of pile shapes, the H-pile showed greater resistance. The close-ended circular pile, however, gave smaller resistance. If H-piles are compared to the other tested piles, the H-piles show higher pile bearing capacity. Similar to the other slenderness ratios 11 and 14, the H-pile has less cross section area, which allows soil to interfere among the pile shape parts. This interference may be a source of increasing the lateral resistance of H-pile where the lateral resistance depends mainly on the lateral contacted area of the pile shape, as demonstrated in Figure 7. The obtained higher pile capacity for longer piles can also be used to support the aforementioned statement. However, Table 3 and figure 8 provides a summary of the findings.

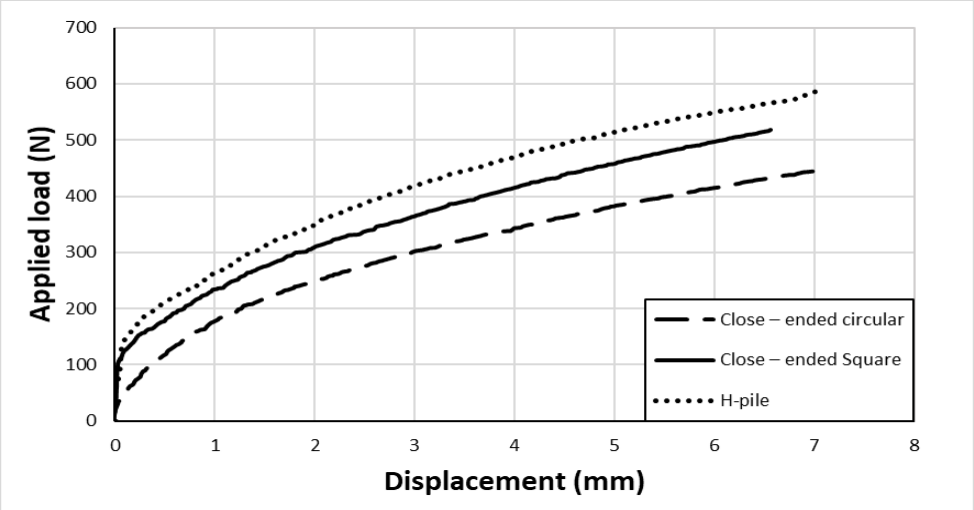

Fig 7. Load- displacement curves for different shapes of piles with L/D =17

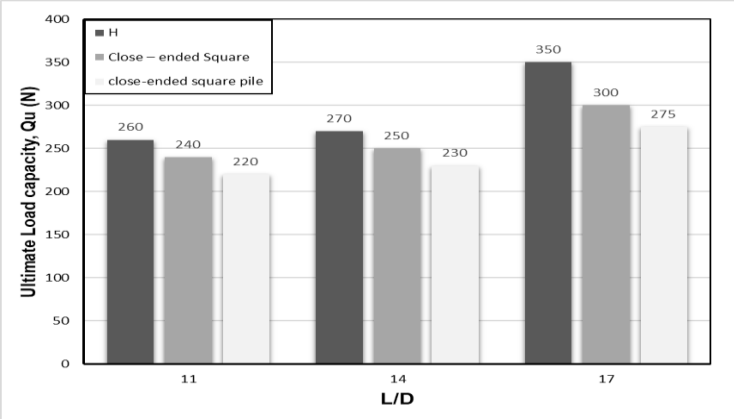

Fig 8. Comparison of various pile lengths and maximum load capacity

TABLE 3. The values of Qu for the piles.

L/D	H-pile (N)	Close-ended Square pile (N)	Close-ended circular pile (N)
11	260	240	220
14	270	250	230
17	350	300	275

To eliminate the units and make the investigation more generic and be applied to other piles, the units have been converted to dimensionless forms, and the symbols used in the current study are defined and presented. The symbol (F) represents a dimensionless form of the failure load divided by the soil unit weight times the pile length cubic. The ratio of perimeter to diameter of pile is presented as (P/D). Figure 9 illustrates the relationship between the form F and perimeter to diameter ratio. It can be realized that with increasing P/D ratio the form F develops for all pile slenderness ratios. This behaviour can be explained by the raising the pile surface area contacted with the surrounding soil.

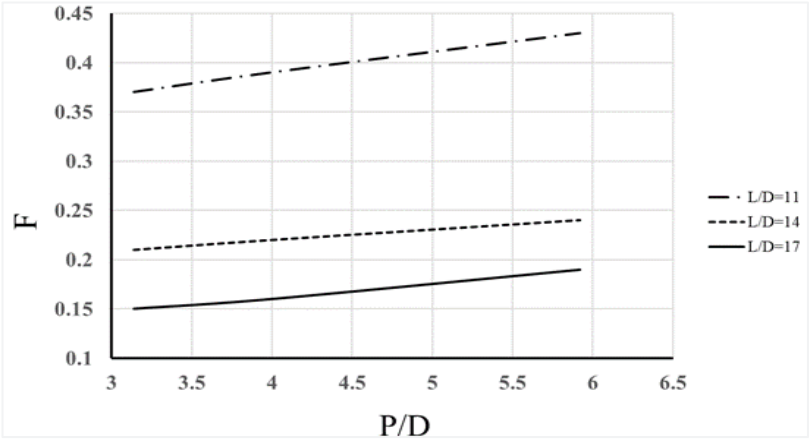

Fig 9. Variation of F versus perimeter to diameter ratio

6.4 Effect of Pile Length

All model piles of various lengths with a constant pile diameter were tested in order to research how pile length affects lateral load capability. Figures 10, 11, and 12 illustrate the impact of pile length on a pile's lateral load capacity with slenderness ratios of 11, 14, and 17. Table 4 presents the capacity for lateral loads of piles with various lengths or different slenderness ratios. From the findings, it is clear that the pile's lateral load capability rises as the pile lengthens. This is because as the length of the pile's embedment increases, the passive resistance becomes active.

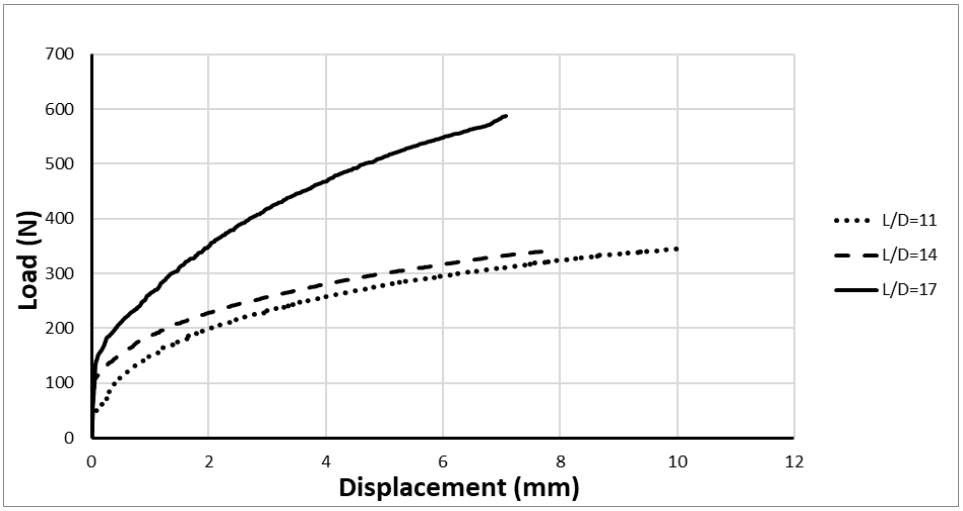

Fig 10: Curves of load- displacement for different H pile lengths

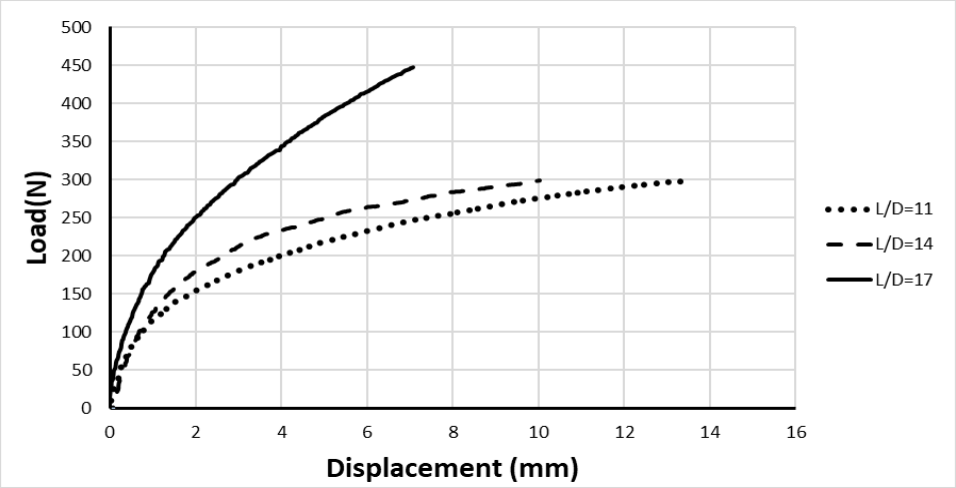

Fig 11. load - displacement curves for different circular pile lengths

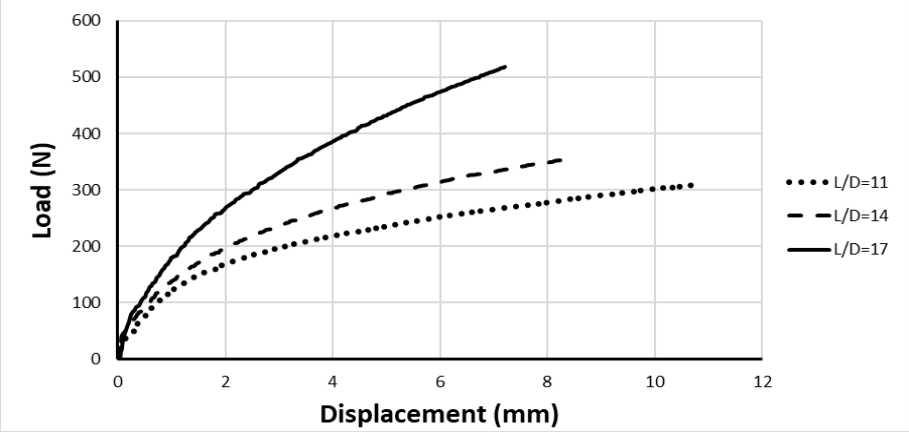

Fig 12. load - displacement curves for different square pile lengths.

TABLE 4. A Pile's Lateral Load Capability of Various Lengths

Pile type	Slenderness ratio	Ultimate lateral load (N)
H-pile	11	260
	14	270
	17	350
Closed-end circular	11	220
	14	230
	17	275
Closed-end square	11	240
	14	250
	17	300

Figure 13 illustrates the relation between the embedded length to diameter ratio of pile and the form F. It is obvious when the slenderness ratio of pile rises, the form F decreases for all pile shapes. This behaviour might be attributed to the symbol F refers to the dimensionless form of the failure load divided by the soil unit weight times the cubic pile length. Therefore, it decreases as the pile length increases.

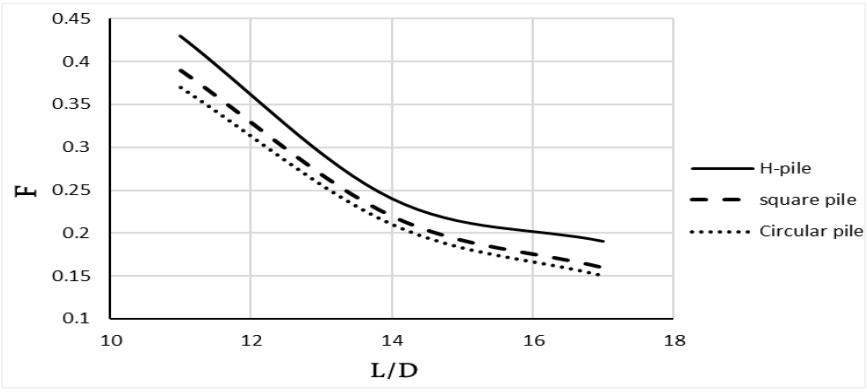

Fig 13. Variation of F versus length to diameter ratio

6.5 Bending Moment Behavior

Figure 14-a displays the strain gauges' distribution attached along the length of the pile. Further, the figure 14-b reveals the usual change in moment of bending along the depth of pile with an L/D ratio of 14 of H-pile, closed end circular and closed end square piles. Based on the findings, it was found that the values of the bending moment along the pile length varied where the maximum value recorded in the upper part of the pile at a length of 170 mm then the values of the bending moment are decreasing by going down of the pile until reaching zero at the pile down end. Thus, the maximum bending moment recorded at depth equals to 42% from the length of the pile. Higher maximum bending moment happens in H-pile is 26.28 N.m and followed by closed end circular pile with 25.14 N.m then closed end square pile of 23.5 N.m.

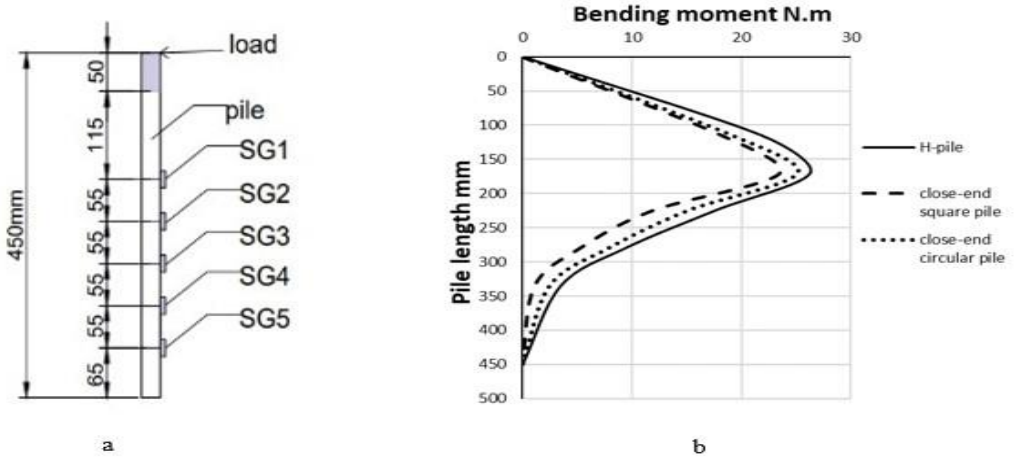

Fig 14. (a) Strain gauges' distribution (dimensions in mm), (b) bending moment distribution of piles

Another presentation of dimensionless forms of parameters involved in this study is revealed in Figure 15. The symbol (M) represents a dimensionless form of the bending moment of pile at failure condition divided by the soil unit weight times the diameter square times pile length square. The ratio of perimeter to diameter of pile is presented as (P/D). The variation of M versus perimeter to diameter ratio is prepared and given below. It can be recognized that the minimum value of M was recorded when perimeter to diameter ratio is about 4 which represent the square pile's bending moment. Thus, the model pile having square cross section records the least bending moment at failure among other studied shapes of piles.

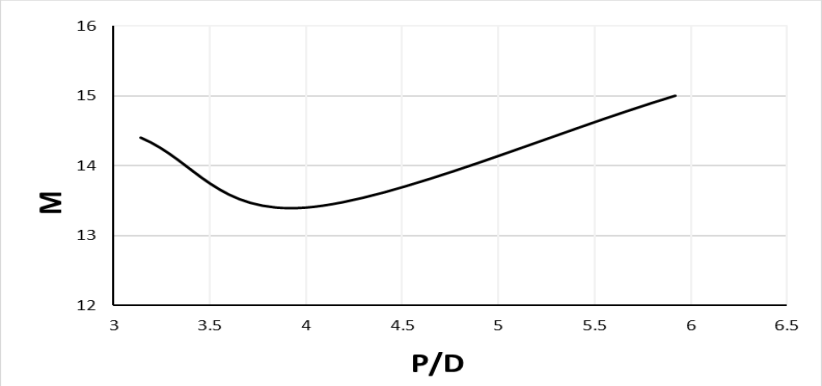

Fig 15. Variation of M versus perimeter to diameter ratio

7 CONCLUSIONs

An experimental study was carried out on single pile having different shapes and lengths with constant diameter. All tests were conducted in sandy soil. Moreover, the bending moment of the pile was obtained using strain gauges attached along the pile. The outcomes of this investigation lead to the following conclusions:

The displacement decreased as the length to diameter (L/D) ratio increase.

The lateral load capacity of the pile increases with increasing the pile embedment length.

When compared to square and circular close-ended piles, H piles showed better strength to the load that is applied.

When the pile's slenderness ratio is 14, the maximum bending moment happened at a depth of 170 mm from the head of pile which represent 42% from the pile's length for all tested pile shapes.

When comparing the value of maximum bending moment of H-pile to closed end square pile is improved by about 1.12 times, while the comparison with closed end circular piles, the development is around 1.05 times.

It can be concluded that the minimum value of M was recorded when perimeter to diameter ratio is about 4 which represent the square pile's bending moment. Thus, the model pile having square cross section records the least bending moment at failure among other studied shapes of piles.

References

1. K. Mahdy, K. A. Kassim, and A. Adnan, “Development of curves of laterally loaded piles in cohesionless soil," the scientific world journal 2014.
2. U. Salini and M. S. Girish, “Lateral load capacity of model piles on cohesionless soil,” Electron. J. Geotech. Eng 14: 1-11, 2009.
3. L. A. Ghabezloo, S. Sulem, J. Randolph, M. F. Kham, and E. Palix, “Pile response to multi-directional lateral loading using P–y curves approach,” Géotechnique, 71(4), 288-298, 2021.
4. S. Mahmoud, A. M. Radwan, M. B. Anwar, “Behaviour of piles subjected to lateral forces in cohesive soil,” 171:260-268.doi: 10.21608/ERJ.2021.194789, 2021.
5. L. Luan, L. Gao, G. Kouretzis, X. Ding, H. Qin, and C. Zheng, “Response of pile groups in layered soil to dynamic lateral loads,” Computers and Geotechnics 142: 104564, 2022.
6. M. Taha, K. Mohammed, A. Al-Neami, and F. H. Rahil. “Experimental and Numerical Study on the Winged Pile-Soil Interaction under Lateral Loads,” IOP Conference Series: Earth and Environmental Science. Vol. 961. No. 1. IOP Publishing, 2022.

7. C. Jiang, L. Liu, J. He, H. Xie, "Effect of the proximity of slope and pile shape on lateral capacity of piles in clay slopes," European Journal of Environmental and Civil Engineering 27, no. 1: 16-30, 2023.
8. N. Begum and K. Muthukkumaran, "Experimental investigation on single model pile in sloping ground under lateral load," International Journal of Geotechnical Engineering 3, no. 1: 133-146, 2009.
9. Z. H. Chik, J. M. Abbas, M. R. Taha, and Q. S. M. Shafiqu, "Lateral behavior of single pile in cohesionless soil subjected to both vertical and horizontal loads," European Journal of Scientific Research 29, no. 2: 194-205, 2009.
10. ASTM, 2000, D 2216 98, Standard Test Method for Laboratory Determination of Water (Moisture) Content of Soil and Rock by mass.
11. ASTM D1556-07 Standard Test Method for Density and Unit Weight of Soil In Place By The Sand-Cone Method.
12. ASTM D422-2000, "Standard Test Method for Particle Size Analysis of Soils", American Society for Testing and Materials.
13. ASTM International - ASTM D698-07 Standard Test Methods for Laboratory Compaction Characteristics of Soil Using Standard Effort.
14. ASTM D3080. (2014). Standard Test Method for Direct Shear Test of Soils under Consolidated Drained Conditions. Philadelphia, PA: American Society of Testing Materials.
15. ASTM D4254. (2014). Standard Test Methods for Minimum Index Density and Unit Weight of Soils and Calculation of Relative Density. Philadelphia, PA: American Society of Testing Materials.
16. ASTM D854-2005, "Standard Test Method for Specific Gravity of Soil Solids by Water Pycnometer", American Society for Testing and Materials.
17. M. D. Bolton, M. W. Gui, J. Garnier, J. F. Corte, G. Bagge, J. Laue, and R. Renzi, "Centrifuge cone penetration tests in sand," Géotechnique 49, no. 4: 543-552, 1999.
18. M. F. Al-Zrejawi, "Performance of Pile Foundations under Axial Loading for Cohesive Soil," M. Sc. thesis, University of Kufa, 2022.
19. H. G. Poulos, and E. H. Davis, "Pile foundation analysis and design" (Vol. 397). New York: Wiley, 1980.
20. ASTM D 4643-17. "Standard test method for determination of water content of soil and rock by microwave oven heating," 2017.
21. M. N. Som and S. C. Das, "Theory and practice of foundation design" PHI Learning Pvt. Ltd., 2003.